Investigating the void structure of the polyamide active layers of thin-film composite membranes

Lin Lin[a], Rene Lopez[b], Guy Z. Ramon[c], Orlando Coronell[a,*]

[a]Department of Environmental Sciences and Engineering, Gillings School of Global Public Health, University of North Carolina at Chapel Hill, Chapel Hill, NC 27599-7431
[b]Department of Physics and Astronomy, University of North Carolina at Chapel Hill, Chapel Hill, NC 27599-3255
[c]Department of Civil and Environmental Engineering, Technion – Israel Institute of Technology, Technion City, Haifa, Israel

* Corresponding author [tel:+1-919-966-9010; fax:+1- 919-966-7911; e-mail: coronell@unc.edu]

Abstract: The potential presence of voids in the fully-aromatic polyamide active layers of thin-film composite (TFC) membranes for water purification was studied in a selection of commercial membranes with a broad range of performance levels. The membranes were characterized for their potential void fractions using three independent methods: (i) analysis of transmission electron microscopy (TEM) images of membrane cross-sections, (ii) water uptake measurements by quartz crystal microbalance (QCM), and (iii) estimates of the effective refractive indices of active layers by spectroscopic ellipsometry. Results revealed that voids having tens of nanometers in diameter exist in the fully-aromatic polyamide active layers of TFC membranes, the voids fill up with water when immersed in it, and the voids account for a significant volume fraction of the active layers (i.e., 15-32% for the membranes studied). It was concluded that the voids in polyamide active layers do not form passageways connecting the feed and permeate sides, but rather are cavities disconnected from the feed side. In addition, it was also concluded that the globular features observable in TEM images of membrane cross sections that had been previously identified as voids or nodules are indeed voids, and not nodules. The finding that a significant volume fraction of fully-aromatic polyamide active layers corresponds to water-filled voids has deep implications on various aspects of TFC membrane science and technology. For example, we illustrate how the presence of voids can potentially increase the *effective* water

permeability of the active layer by as much as a factor of ≈5 compared with the case of an equivalent active layer without any voids. The methods developed in this study to measure void volume fraction represent useful tools for future membrane characterization studies, and the void fractions measured can be used as input or calibration parameters in future modeling studies of active layer formation or water and solute transport.

Key Words: reverse osmosis; aromatic polyamide; active layer; voids; nodules

1. Introduction

Thin-film composite (TFC) membranes with polyamide active layers are used in a broad range of applications, including water desalination, hardness removal, and water reuse by nanofiltration (NF) and reverse osmosis (RO), and energy production [1–4]. Polyamide TFC membranes consist of a top ultrathin (~20-200 nm) polyamide active layer, a microporous polysulfone support (~20-50 μm), and a polyester backing layer (~50-150 μm) [5–7]. The polyamide active layer constitutes the selective barrier to water and solute permeation [5,8], and thus the physical structure of the active layer likely plays an essential role in the water permeability and solute rejection properties of the membranes [9].

The polyamide active layer of TFC membranes has traditionally been assumed to be a dense polymer phase, with pores, if any, no larger than a few nanometers in diameter. This conceptualization of the active layer is reflected in the two mechanistic models commonly used to describe water and solute permeation through polyamide membranes, the solution-diffusion model [10] and the pore-flow model [11]. The solution-diffusion model assumes that the active layer is dense without any pores [10], and the pore-flow model assumes the existence of nanopores (typically cylindrical with a diameter of a few nanometers or less) that stretch across the active layer within an otherwise dense structure [11,12]. Contrary to this conceptualization of the active layer, recent studies [13–16] suggest that globular features visible in cross-sectional transmission electron microscopy (TEM) images of membrane active layers correspond to voids (i.e., regions without polymer) having tens of nanometers in diameter. It is important to note that the voids suggested in these studies are not the same as the pores in the pore-flow model, as the pores in the pore-flow model connect the feed side and permeate side of membrane active layers and have diameters of a few nanometers while the voids apparently seen in the TEM images do

not seem to connect the feed side and permeate side of membrane active layers and have diameters of as much as tens of nanometers.

A different interpretation of the globular features observed in cross-sectional TEM images of polyamide active layers was proposed by Pacheco et al. [17] who indicated that these features correspond to polymer nodules. Based on TEM images of the active layer of a brackish water reverse osmosis (RO) membrane in which globular features 20-60 nm in size were visible, Pacheco et al. further proposed that active layers are composed of a dense nodular base from which the ridge-and-valley structure extends outwards. Similar features to those interpreted as nodules by Pacheco et al. and voids by others [13–16] are visible in TEM images reported elsewhere [18–20], although they were not identified as nodules or voids.

While there is no agreement in the peer-reviewed literature on whether the globular features in TEM images discussed here are voids or dense nodules [21], the features are significantly lighter in shade than the rest of the active layer when bright-field imaging is used [14–20], indicating that they have a lower electron density than the surrounding polymer. Therefore, these features are likely voids, instead of dense nodules, or correspond to regions of significantly lower polymer density. The postulation that the features are voids is supported by the recent scanning electron microscopy (SEM) work by Yan et al. [22] who reported cross-sectional SEM images with features interpreted as voids with sizes of tens to over a hundred of nanometers in diameter. The lack of agreement on whether the globular features are voids or nodules is partially based on the fact that the only evidence supporting either claim are the electron microscopy images themselves which may be affected by the electron beam irradiation during TEM and SEM analysis. If these globular features represent a significant volume fraction of the active layers and are commonly found in fully-aromatic polyamide TFC membranes with a broad range of

performance levels, confirming that they are indeed voids would have important implications for the understanding of transport mechanisms of water and contaminants through polyamide membranes since, as described above, current transport models do not account for voids. Confirming the existence of voids and measuring the volume fraction they account for in polyamide active layers would not only provide a more accurate understanding of active layer structure but also enable a more accurate interpretation of active layer characterization data, e.g., partition and diffusion coefficients in polyamide. The confirmation of the existence of voids as common features in the fully-aromatic polyamide active layers of TFC membranes would also indicate to membrane developers that the voids are an active layer property that could potentially be targeted for optimization towards the development of improved membranes.

Accordingly, the objectives of this study were to evaluate whether (1) the globular features observed in the TEM cross-sectional images are in fact voids, (2) voids exist in a broad range of fully-aromatic polyamide TFC membranes, (3) voids account for a significant volume fraction of the active layers, and (4) voids are filled with water when the membranes are immersed in it. An additional objective was to (5) briefly illustrate some of the implications of the existence of water-filled voids on broad aspects of RO/NF membranes science and technology, with an emphasis on the determination of the water transport properties of polyamide active layers. To accomplish these objectives, a broad range of fully-aromatic polyamide TFC membranes were studied, the volume fractions accounted for by the globular features in the active layers were measured by TEM image analyses, and the volume fractions accounted for by voids in the active layers were measured using two non-microscopy techniques - quartz crystal microbalance (QCM) measurements of water uptake by polyamide active layers and spectroscopic ellipsometry estimates of the refractive indices of active layers. The volume fractions obtained

for the globular features through TEM image analyses and voids through QCM and ellipsometry analyses were compared to each other. Similar volume fractions obtained with the different analyses methods would provide evidence in support of the hypothesis that the globular features are actually voids, not nodules, as the methods employed are based on completely different physical principles. Furthermore, elemental mapping of membrane cross sections using energy dispersive X-ray spectroscopy and electron energy loss spectroscopy were also used to evaluate the elemental composition of the globular features so as to ascertain their void or nodular nature. QCM measurements also served to assess whether the voids filled up with water. This study presents experimental results and their corresponding discussion, as well as the implications of the findings to the study and development of polyamide TFC membranes.

2. Materials and Methods

2.1. Target membranes and sample preparation

Five fully-aromatic polyamide TFC membranes of various performance levels were studied: NF90 [23], XLE [24] and SW30HR [25] received as flat sheets in dry state (Dow Filmtec, Minneapolis, MN) and ESPA3 [26] and SWC4+ [27] received as flat sheets in wet state (Hydranautics, Oceanside, CA). ATR-FTIR analyses (see Section S1 in Supplementary Material) indicated that all membranes have aromatic polyamide active layers and that the active layer of the SW30HR membrane has a coating, which is likely polyvinyl alcohol [28]. Membrane samples were initially prepared as 2.5×5.0 cm^2 coupons thoroughly rinsed with and stored in ultrapure water (>18 MΩ·cm). Before further sample preparation for TEM, QCM, ellipsometry and atomic force microscopy (AFM) analyses, the coupons were blot-dried by placing them between two filter paper circles (qualitative grade circles No.1, 9 cm in diameter,

Whatman) and applying fingertip pressure [29,30]. Pressure exerted in this manner is orders of magnitude lower than the pressure that RO/NF membranes experience during membrane operation in treatment plants (~100-1,200 psi). The coupons were then air dried overnight.

2.2. TEM analyses

For TEM analyses, a membrane sample preparation procedure similar to that described by Tang et al. [18] was used. In brief, membrane samples were dehydrated with 100% ethanol, infiltrated and embedded with LR White resin (London Resin Co., Reading, UK) diluted in ethanol, cured at 48°C for 3 days, and cut into thin (~90-100 nm) slices with a Sorvall MT 6000 Ultramicrotome (RMC Co., Tucson, AR). TEM imaging of membrane cross-sections was performed with a JEOL 100CX II TEM (JEOL USA, Peabody, MA) at an acceleration voltage of 80 kV. Three images were taken for each membrane studied at magnifications of 29,000× or 72,000× depending on the thickness of the active layers. Control TEM images were obtained for SWC4+ membrane samples dried using supercritical CO_2 drying, which confirmed that air/ethanol drying did not affect the active layer structure (see Section S2 in Supplementary Material).

2.3. Scanning transmission electron microscopy-energy dispersive X-ray spectroscopy (STEM-EDS) and electron energy loss spectroscopy (STEM-EELS) analyses

Membrane sample preparation and sectioning for STEM-EDS and STEM-EELS analyses were performed in the same manner as for TEM analyses. STEM-EDS and STEM-EELS analyses of SWC4+ membrane samples were performed with an aberration corrected scanning transmission electron microscope (STEM) FEI Titan (FEI, Houston, TX) at an acceleration voltage of 200 kV and magnification of 80,000×. The Titan was equipped with a SuperX EDS system with four

Bruker silicon drift detectors (Bruker AXS, Madison, WI) and a Gatan Enfinium spectrometer with high-speed spectrum imaging (Gatan Inc., Pleasanton, CA). Multiple locations on SWC4+ sample cross-sections were analyzed.

2.4. SEM analyses

Membrane coupons were removed from the ultrapure water and gently shaken twice to remove excess water. Next, the samples were immersed in liquid nitrogen for 30 seconds, taken out and cracked in air. Secondary electron SEM imaging of membrane cross-sections was performed with a FEI Helios 600 Nanolab Dual Beam System after the samples were coated with a thin film (<5 nm) of Au (60%):Pd (40%) (Ted Pella, Redding, CA) using a Cressington 108 Auto Sputter Coater (Cressington Scientific Instruments, Watford, UK). Triplicate images were taken for each membrane studied at magnifications of 40,000×, 60,000× or 80,000× depending on the thickness of the active layers.

2.5. Active layer isolation

Membrane active layers were isolated onto gold-coated QCM sensors and silicon wafers for ellipsometry and AFM analyses. The active layer isolation procedure was similar to that described in our previous study [31], is based on a protocol previously reported by Freger [32], has been successfully used by various research groups [7,17,22], and has been shown not to affect physico-chemical and transport properties of the active layer [31,33]. Briefly, the membrane polyester backing was peeled off by hand leaving behind a composite of the polyamide active layer and polysulfone support layer. Next, the polyamide-polysulfone composite was placed on a clean sensor/wafer, with the active layer facing the sensor/wafer and the sensor/wafer resting on top of a customized stainless steel support. A matching customized

stainless steel frame with an open window in the center was used to secure the composite and sensor/wafer to the metal support. Then, dimethylformamide (DMF) (Fisher Scientific, Pittsburgh, PA) was added in a dropwise manner through the metal frame window to dissolve the polysulfone layer and the DMF-polysulfone solution was discarded after 1 min. This process was repeated 15 times, after which the assembly was air dried. Next, the sensor/wafer with the active layer already isolated onto it was removed from the metal assembly and the isolated active layer was left in air overnight for further drying. In order to remove any polysulfone remaining on the sample, the sensor/wafer coated with the active layer was dipped in fresh DMF for 4 h and air dried overnight. The sample was finally rinsed with ultrapure water and gently dried with ultrapure nitrogen gas. Any potential gaps created between the isolated active layers and sensor/wafer surfaces due to the roughness of the membrane surface were shown not to affect the active layer void fractions estimated from QCM and ellipsometry analyses (see Section S6 in Supplementary Material).

2.6. QCM analyses

A Q-Sense E4 QCM (Biolin Scientific, Lithicum Heights, MD) was used to measure the areal mass ($ng \cdot cm^{-2}$) of active layer polymer isolated on QCM sensors and the areal mass of water absorbed by active layers. For each membrane, we tested two samples, each with an area of 1.54 cm^2, and for each sample we conducted duplicate measurements of water sorption in each liquid and vapor environments. The mass of active layer isolated on a sensor (m_{AL}) was obtained as described in our previous study [31] from the difference in QCM response between the uncoated sensor and the sensor coated with the active layer. Active layer mass measurements were performed with the sensors placed in Q-Sense flow modules (Biolin Scientific, Lithicum

Heights, MD), which are depicted in Figure 1a. During measurements the sensors were exposed to air in the absence of flow.

Water uptake in liquid environment (m_l) was obtained from the difference in QCM response to the coated sensor exposed to dry nitrogen (<0.02% relative humidity-RH) and to ultrapure water. Measurements were performed with the sensors placed in Q-Sense flow modules (see Figure 1a). During measurements with liquid water, the surface of the sensors was in direct contact with the water. The water flow rate (0.1 $mL \cdot min^{-1}$) was adjusted to ensure laminar conditions and negligible disturbance of the sensor. Each of the dry nitrogen gas and liquid water streams were allowed to flow until the system reached equilibrium (typically 10-20 min), as indicated by a rate of change in areal mass lower than 3.6 $ng \cdot cm^{-2} \cdot min^{-1}$. This parameter was chosen as an indicator of equilibrium for water uptake tests with both liquid water and humidified nitrogen gas because 3.6 $ng \cdot cm^{-2} \cdot min^{-1}$ is 2-3 orders of magnitude lower than the rates of change in areal mass measured in the first few minutes of exposure of the active layers to either fluid, and because 3.6 $ng \cdot cm^{-2}$ corresponds to <0.08% and <0.2% of the water sorption values measured under liquid water and humidified nitrogen, respectively.

Water sorption in vapor environment (m_v) was obtained from the difference in QCM response to the coated sensor exposed to dry nitrogen and to humidified nitrogen gas at 96% RH. Measurements were performed with the sensors placed in Q-Sense humidity modules (Biolin Scientific, Lithicum Heights, MD), which are depicted in Figure 1b. The humidity modules had two chambers separated by a GORE^{TM} membrane (W. L. Gore & Associates, Newark, DE). While the dry and humidified nitrogen streams flowed through the 'outer' chamber (<0.1 psi), the sensor surface was in contact with the 'inner' chamber. Each of the dry and 96% RH

(a) QCM module for testing water sorption in liquid water

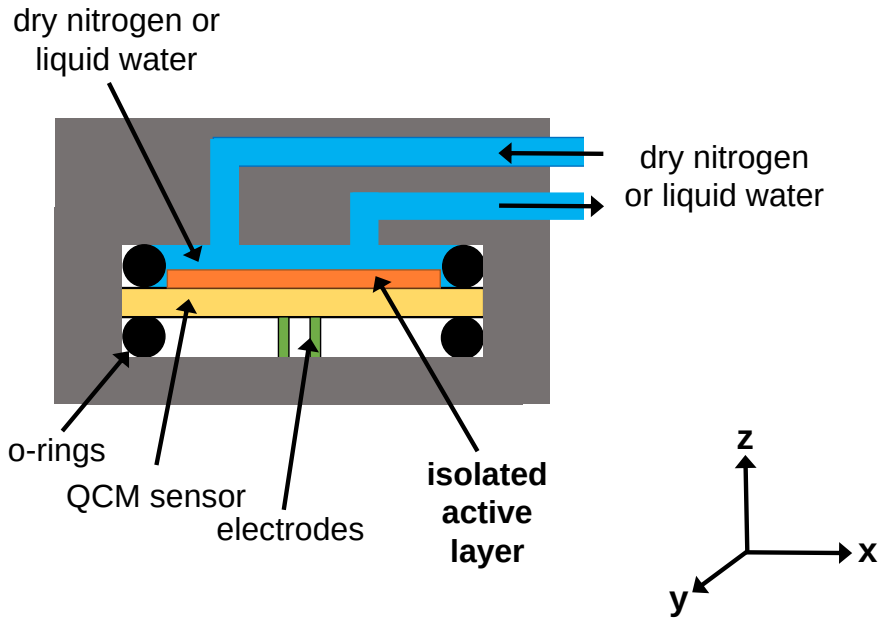

(b) QCM module for testing water sorption in humidified nitrogen gas

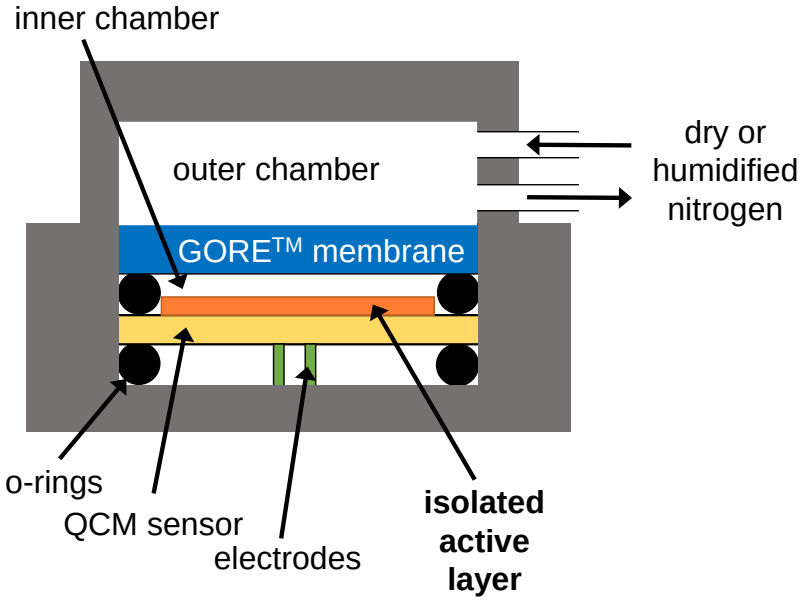

Figure 1. Schematic of a cross section of the quartz crystal microbalance (QCM) modules used for water uptake tests. (a) Flow module for measurement of water uptake by active layers when exposed to liquid water. The flow module was also used for measurement of active layer mass with the sensors exposed to air in the absence of flow. (b) Humidity module for measurement of water uptake by active layers when exposed to humidified nitrogen gas. The schematics are not to scale. In the schematics, the positioning of the inlet and outlet channels of the modules have been slightly modified for clarity; in reality they are located on the same *xy* plane.

nitrogen streams were allowed to flow through the outer chamber until the outer chamber-inner chamber-active layer system reached equilibrium, as indicated by our indicator of equilibrium described above, i.e., a rate of change in areal mass lower than 3.6 $ng \cdot cm^{-2} \cdot min^{-1}$. The 96% RH level in the nitrogen stream was achieved by flowing dry nitrogen through cylinders filled with water and verifying the relative humidity of the exit stream with a humidity meter. Humidified nitrogen gas at 96% RH was used to prevent water condensation during experiments (i.e., at 96% RH, dew point is 21°C).

In all cases, an uncoated control sensor was exposed in parallel to the same liquids or gases as the coated sensors to account for changes in the response of the QCM due to variations in the viscosity and density of the fluid to which the sensor was exposed, as well as to surface adsorption to the sensor and isolated active layer [31,34,35]. In other words, the measurements obtained with the control bare sensor were always subtracted from those obtained with the isolated active layer sample (e.g., m_l or m_v = apparent mass increase in active layer sample – apparent mass increase in control bare sensor). All experiments were performed at a temperature of 22±0.05°C using the temperature control feature of the QCM.

2.7. Ellipsometry analyses

The refractive indices of the membrane active layers were obtained using spectroscopic ellipsometry. Samples consisted of active layers isolated on silicon wafers. In spectroscopic ellipsometry, the relative amplitude and phase changes between two orthogonal polarizations of a light beam reflected off the sample under study are measured as a function of light wavelength and incidence angle. This information is then fitted to an electromagnetic model of the sample, leaving the unknown properties or geometrical features (in this case the active layer refractive

index and thickness) as adjustable parameters. The particular way in which the refractive index is a function of the light wavelength is referred to as "dispersion formulae". "Cauchy" formulae is the simplest dispersion used, and it is particularly suitable to describe the optical properties of weakly absorbing materials [36] such as various transparent polymers [37–39]. Therefore, our complete model used to fit the ellipsometric data consisted of a 3-layer structure having a Cauchy layer at the surface representing the active layer, an intermediate 2-nm silicon dioxide layer [40], and 1-mm silicon substrate. Triplicate samples were analyzed for each membrane, and three locations (0.3 cm^2 each) were analyzed in each sample using a variable angle spectroscopic ellipsometer (J.A. Woollam Co., Lincoln, NE). Data acquisition was performed at incidence angles of 65°, 70° and 75° and wavelength range of 380-1000 nm using the Autoretarder feature. Data analysis was performed using the software WVASE® (J.A. Woollam Co.). Cauchy dispersion formulae [36] were used to describe the optical properties of the polymer layer by selecting the appropriate option in the WVASE® software whose database also contains the well-known optical constants for silicon and silicon dioxide. The refractive index and thickness of the active layers were obtained with the WVASE® software by fitting the data to the model until a minimized mean squared error of less than 20 was reached. This relatively low mean squared error resulted in model simulations matching the experimental data (see representative fitted data in Section S3 in Supplementary Material), therefore indicating that the Cauchy formulae described well the data.

2.8. AFM analyses

Active layer thickness was characterized with an Asylum Research MFP-3D AFM (Santa Barbara, CA) and Tap300Al tips (BudgetSensors, Sofia, Bulgaria) in tapping mode, using a procedure similar to that described by Freger [32]. Briefly, active layers isolated on silicon

wafers were gently scratched with a sharp razor to expose the surface of the wafer and obtain multiple polyamide thin strips. AFM analysis was then used to obtain topography profiles of the thin strips covering areas approximately 30×30 μm^2 in size. The topography profiles allowed the determination of the average thickness of the isolated polyamide film from the difference of the average height of the polyamide surface and the average height of the silicon wafer surface. While we did not detect any polyamide rolling up or separation from the substrate, to avoid any potential confounding edge effects, we did not use in the calculations the data from ≈6-μm wide bands of polymer and substrate next to either edge of the film strips. Triplicate samples of each membrane were analyzed.

2.9. Water permeation tests

Permeation experiments were performed in duplicate for each membrane using a Sterlitech™ (Kent, WA) HP4750 dead-end stirred filtration system (14.6 cm^2 effective membrane area) operated with ultrapure water at 20±2°C and a transmembrane pressure (ΔP) of 0.67 MPa. Permeate volume was measured using an electronic balance and filtration time using a stopwatch until a stabilized water flux (J_v, $m \cdot s^{-1}$) was reached. Under the framework of solution-diffusion theory [10], the water permeability of the active layers was quantified by the water permeability coefficient (A, $m \cdot s^{-1} \cdot Pa^{-1}$) as calculated from

$$J_v = A(\Delta P - \Delta \pi), \quad (1)$$

where $\Delta \pi$ (Pa) is the transmembrane osmotic pressure which was zero in our experiments.

3. Results and Discussion

3.1. Presence of globular features in active layers

Figure 2 shows representative cross-sectional bright-field TEM and SEM images of the NF90, ESPA3 and SWC4+ membranes. Similar images (not shown) were obtained for the XLE and SW30HR membranes. For each membrane, the region corresponding to the active layer is outlined in red dotted lines. For all membranes, the TEM images show well-defined globular features, lighter in color than the surrounding polyamide, similar to the features identified as voids [13–16] and nodules [17] in the literature. The grayscale contrast between any two regions in TEM images is produced by the difference in the amount of electrons of the analysis beam that pass through the two regions of the sample [41]. Areas with lower electron density (i.e., fewer or smaller atoms) allow for the transmission of a higher number of electrons of the analysis beam, resulting in corresponding lighter image areas in bright-field TEM images. Thus, the significantly lighter color of the globular features with respect to the surrounding polymer indicates that they either are voids or correspond to regions with a significantly lower polymer density than the surrounding polyamide.

The color contrast in the secondary electron SEM images in Figure 2 provides an indication of the cross-sectional topology of the membrane samples [41]. Dark areas correspond to depressions (from where secondary electrons generated cannot reach the detector), which are indicative of the existence of voids in the active layer. The SEM images in Figure 2 are consistent with those reported by Yan et al. [22] and show that the active layer cross sections feature distinct depressions of similar size as the globular features observed in the TEM images. This supports the postulation that the active layers are not continuous dense polymer films, but

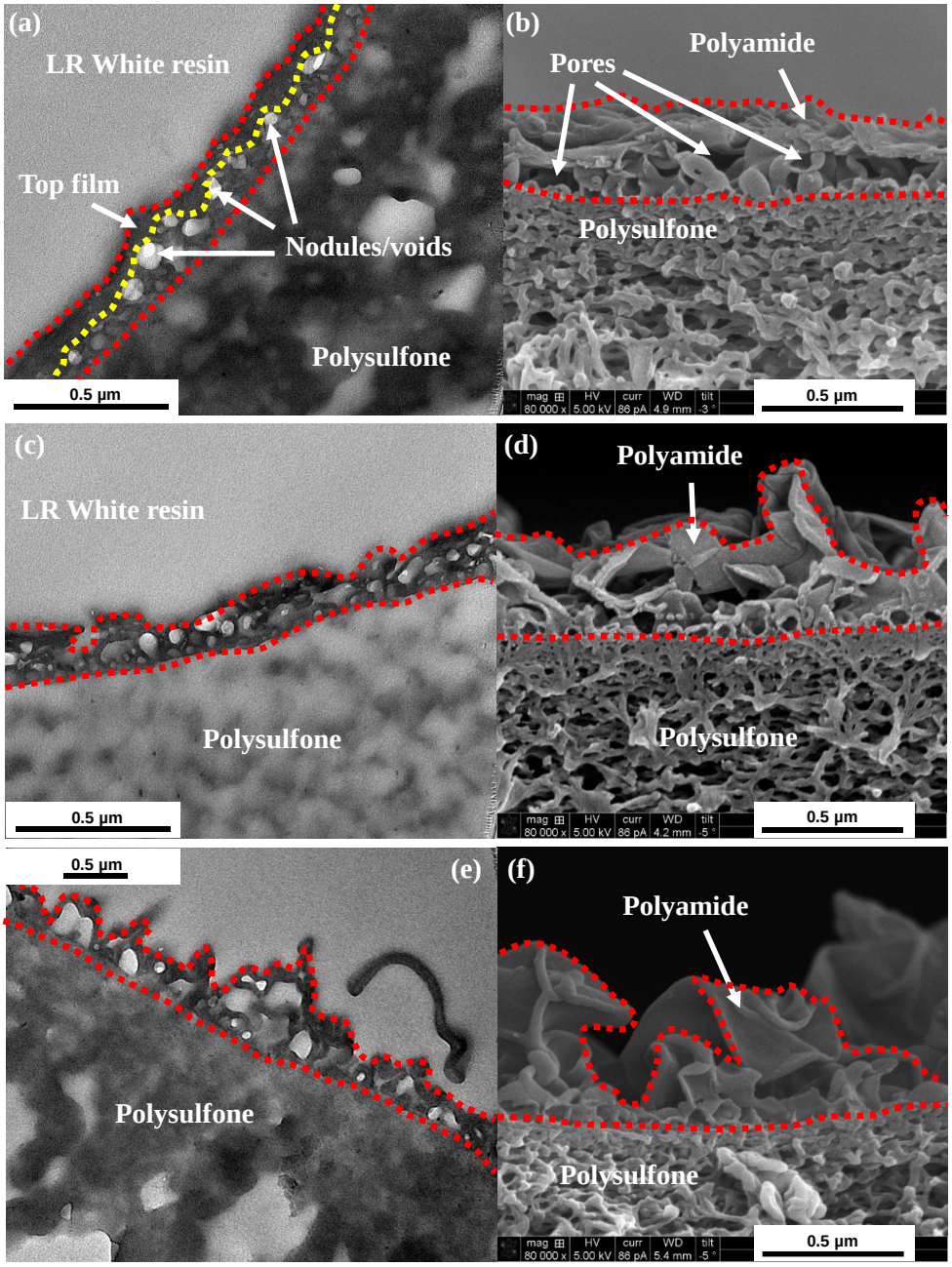

Figure 2. Cross-sectional TEM and SEM images of samples of the (a,b) NF90, (c,d) ESPA3, and (e,f) SWC4+ membranes. For any given membrane, the TEM and SEM images do not correspond to the exact same cross section. The perimeter of the active layers of all membranes is outlined in red dotted lines, and the active layers are labeled in the SEM images. Examples of globular features (i.e., nodules/voids) in the active layers are indicated by arrows for the NF90 membrane. The nodules/voids are also visible in the images of the ESPA3 and SWC4+ membranes. The active layer "top film" is illustrated in the image of the NF90 membrane. The top film refers to the dense (i.e., without voids) active layer region delimited by the active layer surface and the first set of voids from the surface (yellow dotted line).

rather have voids in them. Thus, the TEM and SEM evidence together indicate that the active layer globular features identified as voids by some [13–16,22] and nodules by others [17] commonly exist in polyamide RO and NF membranes of a broad performance range.

3.2. Volume fraction of active layer occupied by globular features from TEM image analyses

Image analysis of the TEM micrographs was performed in order to estimate the volume fractions of the active layers occupied by the globular features. For each TEM image, the software ImageJ 1.47v [42] was used to obtain the area of the active layer and the area of the globular features. The areal fraction of the active layer occupied by the features in a given image ($f_{feature,i}^{areal}$) was calculated as the ratio between the total features area and the total active layer area. It was assumed that for any given membrane, the average areal fraction occupied by the features obtained from arbitrary 2D TEM images was representative of the corresponding 3D volume fraction ($f_{feature}^{volume}$) as given by

$$f_{feature}^{volume} = \left(\frac{1}{m}\right)\sum_{i=1}^{m} f_{feature,i}^{areal}, \qquad (2)$$

where *m* corresponds to the number of TEM images analyzed. The features volume fractions calculated using this approach are shown in Figure 3 as empty bars and were all in the 27-32% range. An analysis of variance (ANOVA) F-test of the results indicates that, with a 95% confidence level, all features volume fractions are *not* statistically different from each other. SEM images were not used to obtain the void fractions because: (1) the cut to obtain the cross sections for SEM (i.e., liquid nitrogen freezing followed by breakage by hand) is not controlled or clean as it is for TEM (i.e., ultramicrotome cut), and (2) it is a very subjective task to

distinguish the polyamide and void regions that are on the focus plane of the SEM image from those that are also visible in the image but are a few/several nanometers behind or before the focus plane.

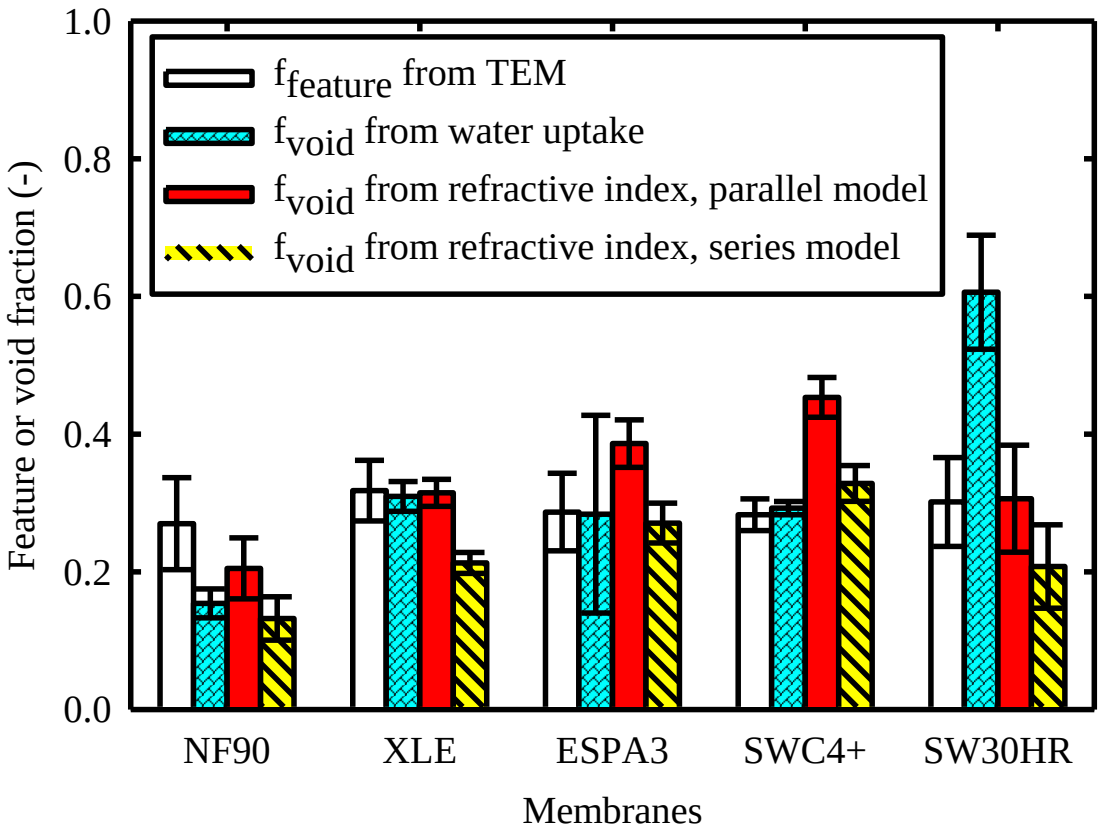

Figure 3. Feature volume fractions ($f_{feature}^{volume}$) and void volume fractions (f_{void}) in the active layers of five commercial polyamide thin-film composite membranes. Feature volume fractions (empty bars) were obtained from analyses of TEM cross-sectional images. Void volume fractions were obtained using (i) water uptake measurements with a QCM and Equation 3 (blue brick bars), and (ii) refractive index estimates by spectroscopic ellipsometry and Equations 4 (parallel model, solid red bars) and 5 (series model, cross hatched yellow bars). For each membrane, the reported values were obtained as follows. The feature volume fraction corresponds to the average of the values obtained for triplicate images. The void volume fraction from water uptake measurements corresponds to the average of the values obtained for duplicate samples (1.54 cm^2 each), where duplicate measurements were taken in each sample. The void fraction from refractive index measurements corresponds to the average of the values obtained for triplicate samples, where three locations (0.3 cm^2 each) were analyzed in each sample. The error bars for the feature volume fractions represent standard deviation. All other error bars represent the propagated error obtained in calculations using the uncertainties in Table 1.

3.3. Void volume fraction from water uptake measurements

Table 1 presents the results for water uptake ($ng \cdot cm^{-2}$) by active layers when exposed to ultrapure water and humidified nitrogen gas at 96% RH. The results show that for all membranes, water uptake was significantly larger (2-5 fold) when the active layer was exposed to liquid water than when it was exposed to humidified nitrogen gas. In terms of thermodynamic equilibrium, if the active layer were a dense polymer phase, the water uptake by the active layer should be the same when exposed to liquid water as when exposed to humidified nitrogen gas at 100% RH (and, by extension, very similar to when exposed to humidified nitrogen gas at 96% RH). This is because both environments represent a water activity of ≈1 outside the active layer, and thermodynamics indicates that it is the water activity outside the active layer, not the water state (i.e., liquid or vapor), that determines the activity of water inside the active layer (see detailed thermodynamic discussion in Section S4 in Supplementary Material). For this reason, other researchers in previous studies [7,43] have also performed water sorption experiments with humidified inert gases at water vapor activities near unity (i.e., 95% RH or 0.95 water activity). The differences observed between the mass changes measured under humidified nitrogen gas and under liquid water were not of a kinetic nature because we ensured that equilibrium was reached for each measurement as detailed in Section 2.6. Thus, the different water uptake results in Table 1 with liquid water from those with humidified nitrogen gas indicate that the active layers are not dense polymer films.

Table 1. Polymer mass (m_{AL}), water uptake in humidified nitrogen (m_v), water uptake in liquid water (m_l), thickness (δ), refractive index at 589 nm (n_{AL}), and active layer top film thickness (δ_{TF}) of membrane active layers.

Membrane	Application	m_{AL} [a,e] (ng·cm^{-2})	m_v [a,e] (ng·cm^{-2})	m_l [a,e] (ng·cm^{-2})	δ [b,f] (nm)	n_{AL} [c,f] (-)	δ_{TF} [d,f] (nm)
NF90	Nanofiltration	17257 ± 128	2163 ± 95	4302 ± 390	120 ± 13	1.56 ± 0.03	35 ± 8
XLE	Brackish water	14060 ± 1065	1763 ± 199	5252 ± 167	136 ± 23	1.48 ± 0.01	40 ± 11
ESPA3	Brackish water	13767 ± 915	1682 ± 7	4872 ± 1732	76 ± 12	1.43 ± 0.02	20 ± 9
SWC4+	Seawater	13415 ± 1588	1868 ± 470	5029 ± 2	113 ± 14	1.38 ± 0.02	42 ± 6
SW30HR	Seawater	18558 ± 842	2309 ± 33	11377 ± 1621	176 ± 25	1.49 ± 0.05	34 ± 18

Notes: [a] Areal masses (m_{AL}, m_v, m_l) were obtained using a QCM from duplicate measurements in each of two samples (1.54 cm^2 each). [b] Active layer thickness (δ) was obtained from AFM analyses of triplicate samples (30×30 μm^2 analysis area in each). [c] Active layer refractive index (n_{AL}) was obtained from ellipsometry analyses of three locations in each of triplicate samples (a total of 9 points per membrane, each point having an area of 0.3 cm^2). [d] Active layer top film thickness (δ_{TF}) was obtained as the product of active layer thickness from AFM analyses (δ) and the ratio between the top film thickness and active layer thickness in triplicate TEM images. [e] Uncertainties represent the difference between the average result for either sample and the average of the two samples analyzed. [f] Uncertainties represent standard deviations.

The larger water uptake from the liquid phase compared with that from the humidified nitrogen gas phase can be explained by the existence of permeable voids within the active layer as depicted in Figure 4. From thermodynamics, when the active layers were exposed to humidified nitrogen gas, both water and nitrogen partitioned into the polyamide phase and saturated the voids. Nitrogen mass uptake by polyamide was negligible because the baseline readings were performed with the active layers exposed to pure dry nitrogen, and the partial pressure (i.e., activity) of nitrogen in humidified nitrogen gas at 96% RH (98,680 Pa) is only 2.6% lower than the partial pressure of nitrogen in pure dry nitrogen (101,325 Pa). Likewise, humidified nitrogen uptake by the voids contributed a negligible mass increase because the densities of dry (1,157 $Kg{\cdot}m^{-3}$) and humidified (1,146 $Kg{\cdot}m^{-3}$) nitrogen gas are within 1% of each other (see calculation of densities in Section S5 in Supplementary Material). Therefore, given that the nitrogen mass uptake by polyamide and humidified nitrogen gas mass uptake by the voids were negligible, then the mass increase measured during tests with humidified nitrogen gas corresponds to the mass uptake associated with water uptake by polyamide (m_v).

As discussed above, water uptake by the polyamide was expected to be the same when the active layers were exposed to liquid water as when they were exposed to humidified nitrogen gas. However, since polyamide is permeable to water, exposure of the active layers to liquid water would also result in water filling the voids. The total mass uptake measured during tests with liquid water (m_l) can therefore be used to calculate the mass uptake associated with the liquid water that filled the voids as $m_l - m_v$. Then the water uptake measurements can be used to calculate the void fraction in active layers (f_{void}) using the expression

$$f_{void} = \frac{total\ void\ volume}{active\ layer\ volume} = \frac{(m_l - m_v)\rho_{AL}}{\rho_w m_{AL}}, \quad (3)$$

where m_l (ng·cm^{-2}) and m_v (ng·cm^{-2}) correspond to the water mass uptake when active layers were exposed to liquid water and humidified nitrogen, respectively, and m_{AL} (ng·cm^{-2}), ρ_{AL}=1.24 g·cm^{-3} [43,44], and ρ_w=1.0 g·cm^{-3} are the active layer polymer mass, effective active layer density (i.e., polymer mass per total active layer volume including polymer and voids), and water density, respectively. Notice that the thickness of the active layer sample analyzed is accounted for by the m_{AL}/ρ_{AL} ratio.

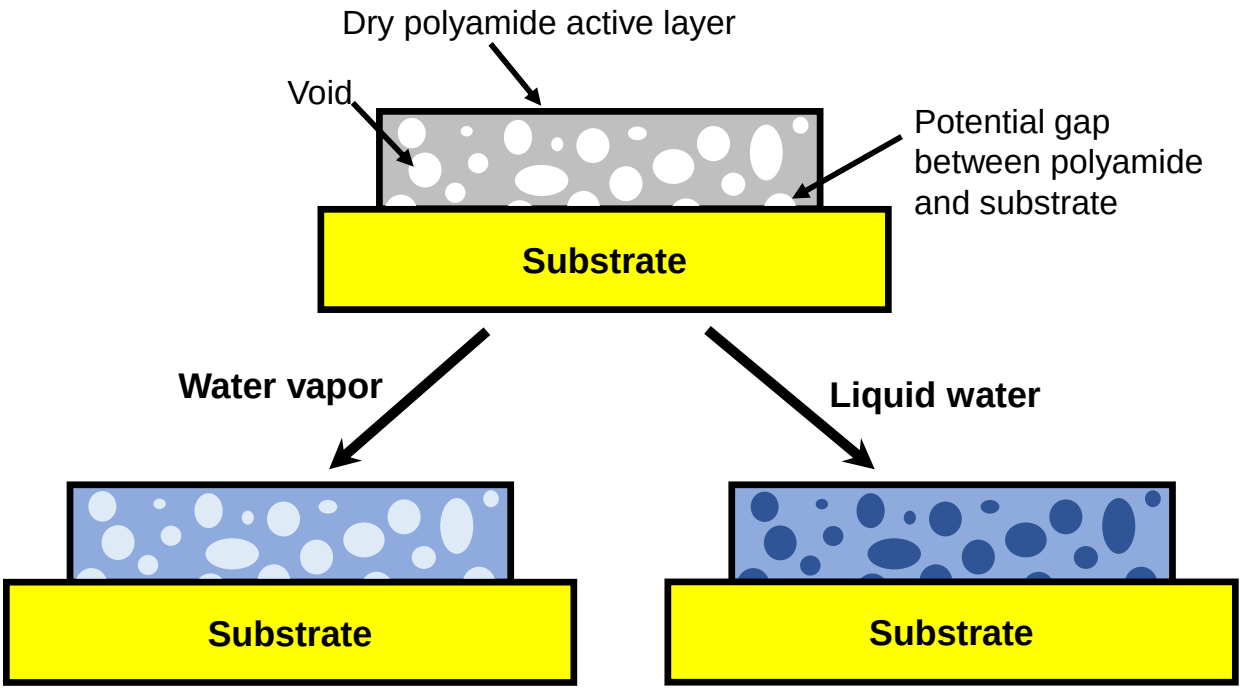

Figure 4. Illustration of an isolated polyamide active layer when exposed to dry nitrogen (top), water vapor via humidified nitrogen gas (bottom left) and liquid water (bottom right). When the active layer is exposed to humidified nitrogen gas, nitrogen and water partition into the polyamide phase and the voids saturate with humidified nitrogen. In contrast, when the active layer is exposed to liquid water, water partitions into the polyamide phase and bulk water, not humidified gas, fills the voids within the active layer. Any potential gaps existing between the isolated active layers and sensor surfaces due to the roughness of the active layer were shown to not affect the active layer void fractions estimated from QCM and ellipsometry analyses. The figure depicts the active layer under the assumption of no interconnectivity between voids, though some void interconnectivity and/or connectivity between voids and the backside of the active layer may exist (see Section 3.5).

Void fractions of the active layers studied were calculated using Equation 3 and the corresponding results are presented in Figure 3 as (blue) brick bars. The volume fractions occupied by the globular features obtained from TEM image analysis and the void fractions calculated from water uptake measurements were compared through Welch's t-tests. Results show that, with a 95% confidence level, the features volume fractions and void fractions are significantly different only for the SW30HR membrane. For the other four membranes, the features volume fractions and void fractions are statistically the same. It is not known why the SW30HR void fraction obtained from water uptake measurements is significantly larger than the features volume fraction obtained from TEM image analyses, but it is reasonable to speculate that it may be related to the PVA coating in its active layer. SW30HR is the only membrane tested that had a coating, and PVA (the coating material) has a significantly higher water absorption (30 wt% [45]) compared to fully-aromatic polyamide (11-20 wt% in the literature [7,43] and 12-14 wt% in this study). Nevertheless, the agreement between the features volume fractions obtained from TEM image analyses and the void fractions obtained from water uptake measurements for all active layers made of only polyamide indicates that the globular features are likely voids, not dense nodules.

Our calculations of void fraction using water uptake measurements have the following uncertainties. In Equation 3, it is assumed that the swelling of active layers in liquid water is the same as in water vapor. While there is no reason to believe that this is not the case, even in the worst-case scenario where no swelling occurred under humidified nitrogen gas but swelling under liquid water were in the 2-35% range reported in the literature for aromatic polyamide active layers [32,46], the error in the void fractions estimated with Equation 3 would be at most 35%. Also, a fraction of the mass increase measured during water uptake tests in both liquid and

humidified nitrogen gas may correspond to the adsorption of water at the external surface of the isolated active layer sample; however, a monolayer of water adsorbed at the external surface (≈30 ng·cm^{-2}) would account for ≈0.6% and ≈1.5% of the measured water uptake in tests with liquid water and humidified nitrogen gas, respectively. Note that the use of a control bare sensor exposed to the same liquids and gases to which the isolated active layer samples were exposed, served to minimize the uncertainties associated with water adsorption to the polyamide surface. Similarly, during measurements with humidified nitrogen gas, capillary condensation may occur in voids having a size smaller than the critical diameter, which was estimated as 30 nm (see Section S7 in Supplementary Material) [47,48]. Based on the size distribution of voids in active layers obtained from TEM images, we estimated that if the kinetics of capillary condensation were such that it occurred to its maximum extent during the timescale of our tests, the fraction of m_v that would be accounted for by capillary condensation would be in the 0-20% range (i.e., 8%, 5%, 20%, 0%, and 5% for the active layers of NF90, XLE, ESPA3, SWC4+, and SW30HR membranes, respectively). This results in a maximum uncertainty -due to capillary condensation- in the f_{void} values calculated with Equation 3 in the 0-7% range (i.e., 4%, 2%, 7%, 0%, and 1% for the active layers of NF90, XLE, ESPA3, SWC4+, and SW30HR membranes, respectively).

Overall, the factor to most likely contribute to uncertainty in our calculations of void fraction with Equation 3 is capillary condensation, which as discussed above is expected to result in an uncertainty of less than 10%. Importantly, we note that capillary condensation can only lead to an underestimation of f_{void} (as m_v would be overestimated in Equation 3). Therefore, even under the uncertainty of possible occurrence of capillary condensation, the results underscore that voids do account for a significant fraction of the volume of active layers.

3.4. Elemental mapping of active layer cross sections

To further evaluate the void nature of the globular features, STEM-EDS and STEM-EELS analyses of SWC4+ membrane cross-sections were performed. Figure 5 shows a representative dark-field STEM image (left), and corresponding nitrogen and sulfur (middle) and carbon (right) STEM-EDS mappings. In the dark-field STEM image, the globules appear as darker regions compared to the surrounding polymer. In the STEM-EDS elemental mappings, dark regions within the red and blue areas correspond to regions where nitrogen content and carbon content, respectively, are significantly lower (or absent) compared to the surrounding polyamide. Similar observations were made in STEM-EELS images (see Figure 6). Therefore, STEM-EDS/EELS images confirm that the globular features are voids or have significantly lower polymer density compared to the surrounding polyamide.

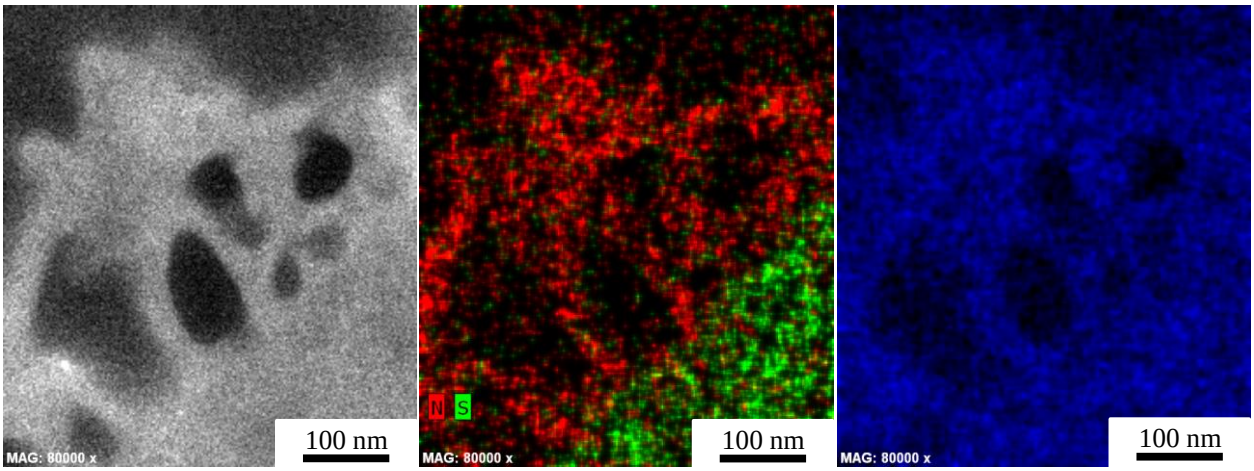

Figure 5. Representative dark-field STEM image (left), and corresponding nitrogen (red) and sulfur (green) STEM-EDS mappings (middle), and carbon (blue) STEM-EDS mapping (right), of a cross section of the active layer of a SWC4+ RO membrane sample. The dark areas within the white (left), red (middle) and blue (right) areas correspond to localized regions where polymer, nitrogen and carbon content, respectively, are significantly lower (or absent) compared to the surrounding polyamide, therefore indicating the presence of a void. In the middle panel, the trace sulfur signal in the polyamide region and trace nitrogen signal in the sulfur region correspond to background signal of the EDS caused by bremsstrahlung radiation.

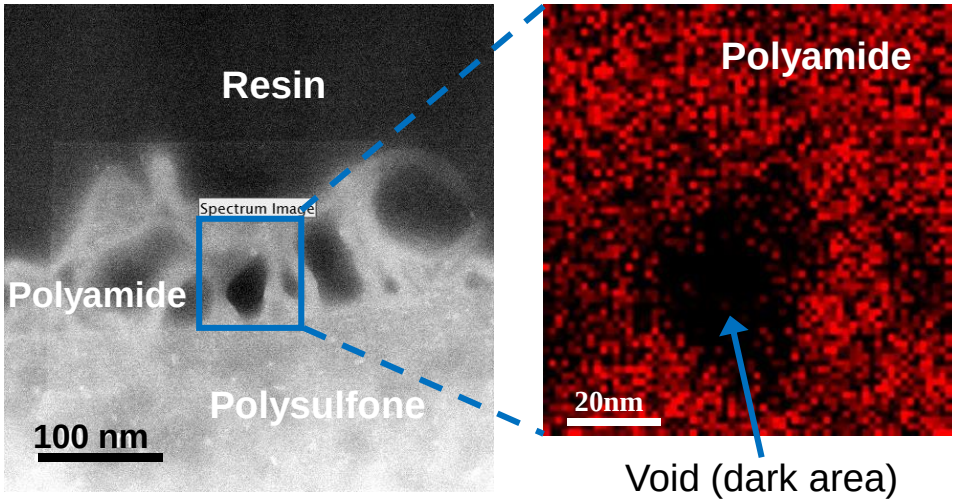

Figure 6. Representative dark-field STEM image (left) and corresponding nitrogen STEM-EELS mapping (right) of a cross-section of the active layer of a SWC4+ RO membrane sample. The red area in the EELS mapping corresponds to regions containing nitrogen which is present in polyamide. The dark area within the red area corresponds to a localized region where nitrogen content is significantly lower (or absent) compared to the surrounding polyamide, therefore indicating the presence of a void.

3.5. Void fraction from refractive indices

Table 1 presents the refractive indices at a light wavelength of 589 nm obtained for the active layers studied by spectroscopic ellipsometry. Assuming that the active layers have voids in them, as supported by the TEM, STEM-EDS/EELS, SEM and QCM results above, one can conceptualize the active layers as a composite having polyamide as the continuous phase and voids as the inclusions that make up the dispersed phase. Therefore, the refractive index measured by ellipsometry constitutes the effective refractive index of the active layer (n_{AL}) and can be related to the refractive indices of polyamide at 589 nm ($n_{polymer}$=1.70) [49] and air (n_{void} =1) [50] filling the voids using effective-medium approximation (EMA) models [51].

EMA models treat heterogeneous media as a homogeneous medium with some effective properties. For the case of a solid-air composite like dry polyamide active layers, the effective properties (e.g., refractive index) are assumed to be independent of the heterogeneity of void size, void size distribution, and spatial distribution of voids. Two of the most commonly used EMA models for the calculation of effective refractive indices are the parallel and series models given by [51]

$$n_{AL} = (1 - f_{void})n_{polymer} + f_{void}n_{void}, \quad (4)$$

and

$$\frac{1}{n_{AL}} = \frac{1-f_{void}}{n_{polymer}} + \frac{f_{void}}{n_{void}}, \quad (5)$$

respectively. These two models cover a wide range of the variability among the refractive index values obtained using the different existing EMA models, with the parallel and series models giving values in the higher and lower ends of the spectrum, respectively [51].

Two other EMA models that are also often used to describe the effective refractive index of interspersed phases are the Maxwell-Garnett and the Bruggeman models [51]. These models assume an arrangement of spheroidal inclusions in the continuous phase, and therefore -from a geometrical perspective- may be considered more appropriate for randomly interspersed phases such as polyamide active layers. Our calculations showed that the void fractions calculated using the parallel, Maxwell-Garnett, and Bruggeman models were not statistically significantly different from each other (see Section S8 in Supplementary Material). As such, we use in our subsequent discussion the f_{void} values calculated with the parallel and series models. The corresponding results are presented in Figure 3 and show that the models provide similar results

when the refractive indices of the continuous and disperse phases are close, such as in our case. We also note that it is not immediately clear which EMA model best describes any particular sample, partly because all models have limitations and there are more than geometrical considerations in their development (e.g., the Maxwell-Garnett and Bruggeman models were initially developed to describe the effective dielectric constant of an interspersed phase, not the effective refractive index, thus inclusions must be significantly smaller than the wavelength of light and be fairly separated) [51].

Welch's t-tests (95% confidence level) were performed comparing the void fractions obtained from ellipsometry analyses using the parallel and series models to the features volume fractions obtained from TEM analyses and the void fractions obtained from water uptake measurements. Results showed that for all possible comparisons (i.e., f_{void} from series model versus $f_{feature}^{volume}$ from TEM results, f_{void} from parallel model versus f_{void} from QCM results, etc.), only one of the membranes (SWC4+) studied had a void fraction obtained from refractive index values that was statistically different from the features volume fraction obtained from TEM images or the void fraction obtained from water uptake tests. The agreement between ellipsometry, TEM and QCM results further supports the existence of voids in the active layers as well as the void nature of the globular features.

3.6. Size and interconnectivity of voids

The existence of voids with diameters >1 nm (including >100 nm) is directly supported by the TEM [13–20] and SEM [13,22] images reported elsewhere, as well as the TEM, STEM-EDS/EELS and SEM images reported in this study. Given that RO/NF membranes have high levels of sodium chloride rejection (i.e., >85% for NF90 [23] and >99% for all others [24–27]),

the existence of voids larger than 1 nm in their active layers indicates that if the voids are interconnected, then the interconnectivity is such that the voids do not form passageways from the feed side to the permeate side. This conclusion is supported by the TEM images in this and other studies [13–20] which show clearly defined voids but not clearly defined passageways from the feed to the permeate side. The lack of interconnectivity between the voids and the feed side is also supported by TEM images in the literature [17,18,52], which show that the filtration of aqueous solutions containing natural organic matter and 10-30 nm gold nanoparticles resulted in natural organic matter and nanoparticle deposition on the active layer surface, not inside the active layer. Finally, note that the absence of connectivity between the voids and the feed side does not exclude the possibility of some level of interconnectivity between voids. SEM images reported by Yan et al. [22] suggest that there is some level of interconnectivity between the voids, and potentially between the voids and the backside of the active layer, but not between the voids and the feed side. Comprehensive characterization of the topology of the voids in polyamide active layer, in particular of the interconnectivity between voids, requires further research and is beyond the scope of this study.

3.7. Broad Implications on RO/NF science and technology

Existing analytical, numerical and atomistic approaches for modeling the transport of water and solutes through RO/NF membranes [9,10,21,44,53–60] and active layer formation [21,44,54–56] do not take into account the existence of voids. Therefore, future transport modeling efforts should evaluate the importance of the presence of voids in active layers (e.g., water/solute partitioning events at polyamide-water interfaces at the voids walls, non-constant water/solute diffusion coefficients in the active layer), and active layer formation modeling efforts should target a more accurate active layer structure that includes the voids. The results from this study

provide quantitative ranges of void volume fractions and sizes that can be used as initial simulation values in transport modeling and calibration values in active layer formation modeling. Also, given that there is no evidence that the voids have been taken into account in membrane optimization efforts, this work reveals to membrane developers that there is an untapped complex parameter (i.e., void size distribution, volume fraction, and topology) that could potentially be optimized to develop improved membranes.

The existing experimental studies in the literature characterizing solute and water transport properties in polyamide active layers (i.e., permeability, partition and diffusion coefficients) have not taken into account the existence of voids [7,29,33,43,61,62]. Therefore, existing studies have assumed that any measurements taken (e.g., water sorption by the active layer) represent the properties of polyamide alone, when they actually represent the effective properties of the polyamide-voids composite (i.e., of the active layer). Thus, future related characterization studies should take into account the presence of the voids in active layers to accurately obtain the transport properties of polyamide and understand the effect that the voids have on the effective properties of the active layer. We elaborate on a related analysis of the water transport properties of polyamide in the next section.

3.8. Implications on analysis of water transport properties of polyamide

3.8.1. Water permeability

Having demonstrated the existence of water-filled voids in fully-aromatic polyamide active layers, we illustrate how accounting for their existence affects the estimated water transport properties of polyamide. In our analysis we take into account void fraction (i.e., amount of

voids) and void interconnectivity, but not other void properties such as size and spatial distribution that may also affect the water transport properties of polyamide.

Under the framework of solution-diffusion theory, the water permeability coefficient A is given by [10]

$$A/\nu = \frac{P_{AL}/\nu}{\delta} = \frac{D_{AL}K_{AL}}{\delta}\frac{C_{Bulk}\nu}{RT} \quad , \tag{6}$$

where P_{AL} ($m^2 \cdot s^{-1} \cdot Pa^{-1}$) is the permeability of the active layer (i.e., an intrinsic property of the active layer material independent of its thickness), δ (m) is the active layer thickness, K_{AL} (-) and D_{AL} ($m^2 \cdot s^{-1}$) are the water partition and diffusion coefficients, respectively, in the active layer, C_{Bulk} is the concentration of bulk water (55.5×10^3 $mol \cdot m^{-3}$), v is the molar volume of water (18.02×10^{-6} $m^3 \cdot mol^{-1}$), R is the ideal gas constant (8.314 $m^3 \cdot Pa \cdot K^{-1} \cdot mol^{-1}$), and T (K) is the absolute temperature. Note that A and P_{AL} are divided by v to convert them from volumetric to molar units. From the traditional perspective that conceptualizes the active layer as a dense polymer film (i.e., f_{void} =0), the active layer permeability (P_{AL}) is interpreted to be the same as the polyamide permeability (P_P) because there are no voids. We calculated P_{AL} values using Equation 6, and the measured δ (Table 1) and A (Table 2) values. The calculated P_{AL} values are presented in Table 2 and were in the $0.2\text{-}2.7 \times 10^{-18}$ $m^2 \cdot s^{-1} \cdot Pa^{-1}$ range. The recognition of the existence of water-filled voids, however, brings the realization that $P_{AL} \neq P_P$ and that P_{AL} actually corresponds to the *effective* permeability of the active layer.

Accurate estimation of P_P requires knowledge of the level of interconnectivity between voids; however, there is currently no technique that allows for the quantitative characterization of void interconnectivity. Therefore, we estimated P_P assuming the two limiting conditions of void

interconnectivity: (i) no void interconnectivity ($P_{P,NI}$), and (ii) complete void interconnectivity ($P_{P,CI}$) including connectivity to the backside of the active layer. The actual polymer permeability thus lies in the permeability range delimited by $P_{P,NI}$ and $P_{P,CI}$.

Under the assumption of no interconnectivity, and using the framework of Maxwell's effective-medium approximation theory [63] in the limit of a large disparity in the diffusion coefficients in the liquid and solid phase (i.e., diffusivity in the liquid in the voids is much bigger than in the solid polyamide), the effective permeability of the active layer P_{AL} is related to the polymer permeability $P_{P,NI}$ and liquid-filled void fraction f_{void} by (see Section S9 in Supplementary Material)

$$\frac{P_{AL}}{P_{P,NI}} = \frac{1+2f_{void}}{1-f_{void}}. \qquad (7)$$

Accordingly, we calculated $P_{P,NI}$ values using Equation 7, and the P_{AL} and f_{void} values in Table 2. We list the resulting $P_{P,NI}$ values also in Table 2.

Under the assumption of complete interconnectivity, the effective active layer thickness is that of the dense (i.e., without voids) active layer region delimited by the active layer surface and the first set of voids from the surface, as illustrated in Figure 2a. We refer to this region as the active layer "top film" and denote its thickness with δ_{TF}. Accordingly, $P_{P,CI}$ can be calculated from

$$A = \frac{P_{P,CI}}{\delta_{TF}}. \qquad (8)$$

The top film thickness δ_{TF} for each of the membranes studied is listed in Table 1 and was obtained as the product of the total active layer thickness obtained from AFM analyses (δ) and the ratio between the top film thickness and active layer thickness in TEM images. We used this

approach because it allowed for a direct comparison of P_{AL} and P_P values, as both P_{AL} and P_P were calculated using thickness values corresponding to the samples analyzed by AFM. AFM measurements are more representative of the actual thickness of the active layers as they correspond to the thickness obtained from samples having 90 μm^2 in size, while TEM images correspond to the thickness obtained from the analyses of only a few (linear) micrometers of sample. We used Equation 8, and the measured δ_{TF} (Table 1) and A (Table 2) values to calculate $P_{P,CI}$ values. We list the resulting $P_{P,CI}$ values in Table 2.

The calculated P_{AL}, $P_{P,NI}$ and $P_{P,CI}$ values listed in Table 2 show that polymer permeability values were lower than corresponding effective active layer permeability values by a factor of 1.5-5.3 (average of 2.9). Thus, the results indicate that the polymer permeability is overestimated by a factor of 1.5-5.3 when the existence of voids is neglected, or equivalently, that the presence of the voids potentially increases the *effective* water permeability of the active layer by as much as a factor of ≈5 compared with the case of an equivalent active layer without any voids.

3.8.2. Water partitioning

A similar comparison between effective active layer properties and polymer properties can be performed for the partitioning of water into polyamide active layers when water sorption measurements are obtained by exposing the active layer to water vapor, as has been done in the literature [7,43]. The *effective* partition coefficient of water into the active layer (K_{AL}) is given by

$$K_{AL} = \frac{C_{AL}}{C_{Bulk}} = \left(\frac{m_v}{MW_W \delta} \right) / C_{Bulk} \ , \qquad (9)$$

Table 2. Permeability coefficient (A), void fraction (f_{void}), active layer effective permeability (P_{AL}), polyamide permeability under the assumption of no void interconnectivity ($P_{P,NI}$), polyamide permeability under the assumption of complete void interconnectivity ($P_{P,CI}$), water partition coefficient in active layer (K_{AL}), water partition coefficient in polyamide (K_P), water diffusion coefficient in active layer (D_{AL}), water diffusion coefficient in polyamide under the assumption of no void interconnectivity ($D_{P,NI}$), and water diffusion coefficient in polyamide under the assumption of complete void interconnectivity ($D_{P,CI}$).

Membrane	$A\times10^{11}$ ($m\cdot s^{-1}\cdot Pa^{-1}$)	f_{void} [a] (-)	$P_{AL}\times10^{18}$ ($m^2\cdot s^{-1}\cdot Pa^{-1}$)	$P_{P,NI}\times10^{18}$ ($m^2\cdot s^{-1}\cdot Pa^{-1}$)	$P_{P,CI}\times10^{18}$ ($m^2\cdot s^{-1}\cdot Pa^{-1}$)	K_{AL} (-)	K_P (-)	$D_{AL}\times10^{9}$ ($m^2\cdot s^{-1}$)	$D_{P,NI}\times10^{9}$ ($m^2\cdot s^{-1}$)	$D_{P,CI}\times10^{9}$ ($m^2\cdot s^{-1}$)
NF90	2.24 ± 0.09	0.15 ± 0.02	2.68 ± 0.31	1.74 ± 0.38	0.78 ± 0.18	0.18 ± 0.02	0.21 ± 0.04	2.01 ± 0.33	1.10 ± 0.31	0.49 ± 0.14
XLE	1.99 ± 0.10	0.31 ± 0.02	2.71 ± 0.47	1.16 ± 0.23	0.80 ± 0.23	0.13 ± 0.03	0.19 ± 0.04	2.83 ± 0.76	0.84 ± 0.24	0.58 ± 0.20
ESPA3	1.48 ± 0.01	0.28 ± 0.14	1.12 ± 0.18	0.52 ± 0.36	0.30 ± 0.13	0.22 ± 0.03	0.31 ± 0.16	0.69 ± 0.15	0.23 ± 0.20	0.13 ± 0.09
SWC4+	0.28 ± 0.03	0.29 ± 0.01	0.32 ± 0.05	0.14 ± 0.02	0.12 ± 0.02	0.17 ± 0.05	0.23 ± 0.07	0.26 ± 0.08	0.08 ± 0.03	0.07 ± 0.02
SW30HR	0.12 ± 0.03	0.30 ± 0.06	0.21 ± 0.06	0.09 ± 0.04	0.04 ± 0.02	0.13 ± 0.02	0.19 ± 0.05	0.21 ± 0.06	0.07 ± 0.03	0.03 ± 0.02

Notes: [a] f_{void} values correspond to those from water absorption measurements, except for the SW30HR membrane for which it corresponds to that obtained using TEM image analysis because the additional water sorbed by the polyvinyl alcohol coating atop the SW30HR membrane does not allow for an accurate estimate of f_{void} from water uptake measurements.

where C_{AL}, MW_W (18.02 g·mol^{-1}), and m_v correspond to the molar concentration of water in the active layer, molar mass of water, and areal mass of water sorbed by the active layer when exposed to a humidified gas at >95% RH. Using Equation 9 and the measured m_v and δ values in Table 1, the calculated K_{AL} values (Table 2) were in the 0.13-0.22 range. Recognizing the existence of voids and remembering that $K_P = C_P/C_{Bulk}$, where C_P corresponds to the molar concentration of water in polyamide, the partition coefficient of water into polyamide (K_P) can be calculated as

$$K_P = \left(\frac{m_v}{MW_W \delta (1 - f_{void})} \right) / C_{Bulk}, \quad (10)$$

because, as described above, the water vapor mass uptake by the voids is negligible and therefore the measured m_v values correspond to the mass water uptake by polyamide. The calculated K_P values using Equation 10 are listed in Table 2. Note that the calculation of water partitioning into polyamide is independent of the level of interconnectivity between pores as it simply depends on the amount of water sorbed by the polymer and the amount of polymer in the active layer. A comparison between the K_{AL} and K_P values in Table 2 indicates that when the voids are neglected, the partition coefficient of water into polyamide is underestimated by a factor of 1.2-1.5 (average of 1.4).

Note that K_{AL} and K_P depend on m_v, and therefore both have the propagated uncertainty from m_v associated with capillary condensation (≤20%). Similarly, while the K_P/K_{AL} = 1.2-1.5 ratio does not directly depend on m_v (i.e., m_v cancels out), it does depend on f_{void} which has a ≤10% uncertainty associated with capillary condensation. Therefore, all calculated parameters that

depend on m_v, f_{void} obtained from water uptake tests, K_{AL} or K_P have an uncertainty associated with the possible occurrence of capillary condensation.

3.8.3. Water diffusivity

The diffusion coefficient of water in the active layer (D_{AL}) calculated using Equation 6 assuming that the active layer is a dense film is presented in Table 2. The results obtained for the NF90 and XLE membranes are not statistically significantly different from the self-diffusion coefficient of liquid water (D_{H2O} =2×10^{-9} m^2·s^{-1}) [64], which suggests that the solution-diffusion model as described by Equations 1 and 6 under the assumption that the active layer is a dense film is likely inaccurate. Diffusion coefficients of water in polyamide under the assumption of no void interconnectivity ($D_{P,NI}$), i.e., $D_{P,NI} = (P_{P,NI}RT)/(K_P C_{Bulk} v)$, and under the assumption of complete void interconnectivity ($D_{P,CI}$), i.e., $D_{P,CI} = (P_{P,CI}RT)/(K_P C_{Bulk} v)$, are also presented in Table 2. The calculated $D_{P,NI}$ and $D_{P,CI}$ values were all well below the self-diffusion coefficient of water. A comparison between D_{AL}, $D_{P,NI}$ and $D_{P,CI}$ values shows that the water diffusion coefficients in the polymer were lower than the effective water diffusion coefficients in the active layers by a factor of 1.8-7.4 (average of 4.0). The results therefore suggest that solution-diffusion theory may satisfactorily explain water permeation in active layers if the voids are taken into account, though a more rigorous modeling approach such as numerical solutions considering two- or three- dimensional flow is likely needed to take into account void topology in the active layer.

4. Conclusions

The presence of voids in the fully-aromatic polyamide active layers of TFC membranes for water purification was studied using a selection of commercial membranes with a broad range of

performance levels. The study was partly motivated by conflicting interpretations in the literature of globular features observed in cross-sectional electron microscopy images of fully-aromatic polyamide TFC membranes that some authors [13–16] have interpreted as voids and some others as nodules [17]. We evaluated the void or nodular nature of the globular features using TEM and SEM imaging as well as STEM-EDS and STEM-EELS elemental mapping, measured the volume fraction of the active layer occupied by the features using TEM image analysis, measured the void volume fraction in active layers using water sorption and refractive index analyses, and illustrated how the voids have an effect on the water transport properties of polyamide and active layers. Our results and discussion support the following conclusions:

- The globular features observed in TEM images are voids, not nodules. This conclusion is supported by (i) the matching volume fractions occupied by the features (TEM image analyses) and volume fraction occupied by voids (water sorption and refractive index analyses) in the active layers, and (ii) the elemental mapping results by STEM-EDS and STEM-EELS.
- The voids are a common feature of fully-aromatic polyamide active layers as they were observed in the active layers of all five fully-aromatic polyamide TFC membranes studied which covered a broad range of performance levels including nanofiltration, brackish water RO and seawater RO.
- Voids accounted for a significant volume fraction (15-32%) of the membrane active layers.
- Voids are filled with liquid water when the membranes are immersed in it.

- The voids in polyamide active layers do not form passageways connecting the feed and permeate sides, but rather are cavities disconnected from the feed side. Further research is required to assess the extent to which the voids are interconnected to each other.
- The presence of the voids increases the effective water permeability of the active layers compared with the case of an equivalent active layer without any voids. For the active layers studied, the potential increase in water permeability was as much as a factor of ≈5.
- Neglecting the presence of the voids led to an overestimation of the water permeability of polyamide by a factor of 1.5-5.3 (average of 2.9), an underestimation of the water partition coefficient into polyamide by a factor of 1.2-1.5 (average of 1.4), and an overestimation of the water diffusion coefficient in polyamide by a factor of 1.8-7.4 (average of 4.0).

In addition to the findings above, this study contributed three different methods to measure void volume fraction in active layers, and experimentally measured void volume fractions that can be used as input or calibration parameters in future modeling studies of water and solute transport or active layer formation. The confirmation of the existence of voids as common features in the fully-aromatic polyamide active layers of TFC membranes indicates that the voids are an active layer property that could potentially be targeted for optimization towards the development of improved membranes.

Acknowledgments

We thank Wallace Ambrose and Amar S. Kumbhar (TEM), Yang Liu (STEM-EDS/EELS), and Carrie Donley (SEM) for assistance in acquisition of microscopy images and helpful discussions. TEM, AFM and ellipsometry analyses were conducted at the Chapel Hill Analytical and

Nanofabrication Laboratory in Chapel Hill, NC. The STEM-EDS/EELS analyses were performed at the Analytical Instrumentation Facility of the North Carolina State University. This work was supported by the National Science Foundation (NSF) Grants Opportunities for Academic Liaison with Industry (GOALI) and Chemical and Biological Separations programs under Award#1264690, and NSF Environmental Engineering program under Award#1336532. G.Z.R was supported by a Marie-Curie grant (No. 275911) from the European Union Seventh Framework Program (FP7/2007-2013).

References

[1] L.F. Greenlee, D.F. Lawler, B.D. Freeman, B. Marrot, P. Moulin, Reverse osmosis desalination: water sources, technology, and today's challenges., Water Res. 43 (2009) 2317–2348. doi:10.1016/j.watres.2009.03.010.

[2] J.G. Jacangelo, R.R. Trussell, M. Watson, Role of membrane technology in drinking water treatment in the United States, Desalination. 113 (1997) 119–127. doi:10.1016/S0011-9164(97)00120-3.

[3] B. Van der Bruggen, K. Everaert, D. Wilms, C. Vandecasteele, Application of nanofiltration for removal of pesticides, nitrate and hardness from ground water: rejection properties and economic evaluation, J. Memb. Sci. 193 (2001) 239–248. doi:10.1016/S0376-7388(01)00517-8.

[4] N.Y. Yip, A. Tiraferri, W.A. Phillip, J.D. Schi, L.A. Hoover, Y.C. Kim, et al., Thin-Film Composite Pressure Retarded Osmosis Membranes for Sustainable Power Generation from Salinity Gradients, Environ. Sci. Technol. 45 (2011) 4360–4369.

[5] R.J. Petersen, Composite reverse osmosis and nanofiltration membranes, J. Memb. Sci. 83 (1993) 81–150. doi:10.1016/0376-7388(93)80014-O.

[6] K.P. Lee, T.C. Arnot, D. Mattia, A review of reverse osmosis membrane materials for desalination—Development to date and future potential, J. Memb. Sci. 370 (2011) 1–22. doi:10.1016/j.memsci.2010.12.036.

[7] J. Lee, C.M. Doherty, A.J. Hill, S.E. Kentish, Water vapor sorption and free volume in the aromatic polyamide layer of reverse osmosis membranes, J. Memb. Sci. 425-426 (2013) 217–226. doi:10.1016/j.memsci.2012.08.054.

[8] C. Bellona, J.E. Drewes, P. Xu, G. Amy, Factors affecting the rejection of organic solutes during NF/RO treatment—A literature review., Water Res. 38 (2004) 2795–2809. doi:10.1016/j.watres.2004.03.034.

[9] G.Z. Ramon, E.M.V. Hoek, Transport through composite membranes, part 2: impacts of roughness on permeability and fouling, J. Memb. Sci. 425-426 (2013) 141–148. doi:10.1016/j.memsci.2012.08.004.

[10] J.G. Wijmans, R.W. Baker, The solution-diffusion model: a review, J. Memb. Sci. 107 (1995) 1–21. doi:10.1016/0376-7388(95)00102-I.

[11] W.R. Bowen, J.S. Welfoot, Modelling the performance of membrane nanofiltration—Critical assessment and model development, Chem. Eng. Sci. 57 (2002) 1121–1137.

[12] A. Szymczyk, P. Fievet, Investigating transport properties of nanofiltration membranes by means of a steric, electric and dielectric exclusion model, J. Memb. Sci. 252 (2005) 77–88. doi:10.1016/j.memsci.2004.12.002.

[13] M. Kurihara, M. Hanakawa, Mega-ton Water System: Japanese national research and development project on seawater desalination and wastewater reclamation, Desalination. 308 (2013) 131–137. doi:10.1016/j.desal.2012.07.038.

[14] Q. An, W.-S. Hung, S.-C. Lo, Y.-H. Li, M. De Guzman, C.-C. Hu, et al., Comparison between Free Volume Characteristics of Composite Membranes Fabricated through Static and Dynamic Interfacial Polymerization Processes, Macromolecules. 45 (2012) 3428–3435. doi:10.1021/ma3001324.

[15] C. Kong, A. Koushima, T. Kamada, T. Shintani, M. Kanezashi, T. Yoshioka, et al., Enhanced performance of inorganic-polyamide nanocomposite membranes prepared by metal-alkoxide-assisted interfacial polymerization, J. Memb. Sci. 366 (2011) 382–388. doi:10.1016/j.memsci.2010.10.026.

[16] C. Kong, M. Kanezashi, T. Yamomoto, T. Shintani, T. Tsuru, Controlled synthesis of high performance polyamide membrane with thin dense layer for water desalination, J. Memb. Sci. 362 (2010) 76–80. doi:10.1016/j.memsci.2010.06.022.

[17] F.A. Pacheco, I. Pinnau, M. Reinhard, J.O. Leckie, Characterization of isolated polyamide thin films of RO and NF membranes using novel TEM techniques, J. Memb. Sci. 358 (2010) 51–59. doi:10.1016/j.memsci.2010.04.032.

[18] C.Y. Tang, Y.-N. Kwon, J.O. Leckie, Probing the nano- and micro-scales of reverse osmosis membranes—A comprehensive characterization of physiochemical properties of uncoated and coated membranes by XPS, TEM, ATR-FTIR, and streaming potential measurements, J. Memb. Sci. 287 (2007) 146–156. doi:10.1016/j.memsci.2006.10.038.

[19] C.Y. Tang, Q.S. Fu, A.P. Robertson, C.S. Criddle, J.O. Leckie, Use of Reverse Osmosis Membranes to Remove Perfluorooctane Sulfonate (PFOS) from Semiconductor Wastewater, Environ. Sci. Technol. 40 (2006) 7343–7349.

[20] J. Yin, E.-S. Kim, J. Yang, B. Deng, Fabrication of a novel thin-film nanocomposite (TFN) membrane containing MCM-41 silica nanoparticles (NPs) for water purification, J. Memb. Sci. 423-424 (2012) 238–246. doi:10.1016/j.memsci.2012.08.020.

[21] H.F. Ridgway, J.D. Gale, Z.E. Hughes, M.B. Stewart, J.D. Orbell, S.R. Gray, Molecular scale modeling of membrane water treatment processes, in: M. Duke, D. Zhao, R. Semiat (Eds.), Funct. Nanostructured Mater. Membr. Water Treat., John Wiley & Sons, Inc., 2013.

[22] H. Yan, X. Miao, J. Xu, G. Pan, Y. Zhang, Y. Shi, et al., The porous structure of the fully-aromatic polyamide film in reverse osmosis membranes, J. Memb. Sci. 475 (2015) 504–510. doi:10.1016/j.memsci.2014.10.052.

[23] Dow Filmtec. NF90-400 nanofiltration element datasheet, Form No. 609-00345-0312. Available at http://www.dowwaterandprocess.com/en/Products/F/FILMTEC%20NF90_4040 (Accessed on October 26, 2014).

[24] Dow Filmtec. XLE-440 extra low energy RO element datasheet, Form No. 609-00245-0606. Available at http://www.dowwaterandprocess.com/en/products/f/filmtec_xle_4040 (Accessed on October 26, 2014).

[25] Dow Filmtec. SW30HR-380 seawater reverse osmosis element datasheet, Form No. 609-00390-1008. Available at http://www.dowwaterandprocess.com/en/products/f/filmtec_sw30hr_380 (Accessed on October 26, 2014).

[26] Hydranautics. ESPA3-4040 brackish water reverse osmosis membrane element datasheet. Available at http://www.lenntech.com/Data-sheets/Hydranautics-ESPA3-4040.pdf (Accessed on October 26, 2014).

[27] Hydranautics. SWC4+ 8040 seawater reverse osmosis element datasheet. Available at http://www.lenntech.com/Data-sheets/Hydranautics-SWC4+8040.pdf (Accessed on August 26, 2015).

[28] C.Y. Tang, Y.-N. Kwon, J.O. Leckie, Effect of membrane chemistry and coating layer on physiochemical properties of thin film composite polyamide RO and NF membranes I. FTIR and XPS characterization of polyamide and coating layer chemistry, Desalination. 242 (2009) 149–167. doi:10.1016/j.desal.2008.04.003.

[29] X. Zhang, D.G. Cahill, O. Coronell, B.J. Mariñas, Partitioning of salt ions in FT30 reverse osmosis membranes, Appl. Phys. Lett. 91 (2007) 181904. doi:10.1063/1.2802562.

[30] O. Coronell, B.J. Mariñas, D.G. Cahill, Accessibility and ion exchange stoichiometry of ionized carboxylic groups in the active layer of FT30 reverse osmosis membrane, Environ. Sci. Technol. 43 (2009) 5042–5048.

[31] L.A. Perry, O. Coronell, Reliable , bench-top measurements of charge density in the active layers of thin-film composite and nanocomposite membranes using quartz crystal microbalance technology, J. Memb. Sci. 429 (2013) 23–33. doi:10.1016/j.memsci.2012.11.023.

[32] V. Freger, Swelling and morphology of the skin layer of polyamide composite membranes: an atomic force microscopy study, Environ. Sci. Technol. 38 (2004) 3168–3175.

[33] S. Bason, Y. Oren, V. Freger, Ion transport in the polyamide layer of RO membranes: Composite membranes and free-standing films, J. Memb. Sci. 367 (2011) 119–126. doi:10.1016/j.memsci.2010.10.048.

[34] K.A. Marx, Quartz crystal microbalance: a useful tool for studying thin polymer films and complex biomolecular systems at the solution-surface interface, Biomacromolecules. 4 (2003) 1099–1120. doi:10.1021/bm020116i.

[35] C.K. O'Sullivan, G.G. Guilbault, Commercial quartz crystal microbalances—Theory and applications, Biosens. Bioelectron. 14 (1999) 663–670. doi:10.1016/S0956-5663(99)00040-8.

[36] E.A. Irene, A brief history and state of the art of ellipsometry, in: M. Losurdo, K. Hingerl (Eds.), Ellipsom. Nanoscale, Springer-Verlag Berlin Heidelberg, 2013: pp. 1–30. doi:10.1007/978-3-642-33956-1.

[37] W. Ogieglo, H. van der Werf, K. Tempelman, H. Wormeester, M. Wessling, A. Nijmeijer, et al., n-Hexane induced swelling of thin PDMS films under non-equilibrium nanofiltration permeation conditions , resolved by spectroscopic ellipsometry, J. Memb. Sci. 431 (2013) 233–243.

[38] O. Kahle, U. Wielsch, H. Metzner, J. Bauer, C. Uhlig, C. Zawatzki, Glass transition temperature and thermal expansion behaviour of polymer films investigated by variable temperature spectroscopic ellipsometry, Thin Solid Films. 313-314 (1998) 803–807.

[39] W. Ogieglo, H. Wormeester, M. Wessling, N.E. Benes, Spectroscopic Ellipsometry Analysis of a Thin Film Composite Membrane Consisting of Polysulfone on a Porous α-Alumina Support, Appl. Mater. Interfaces. 4 (2012) 935–943.

[40] Y. Huang, D.R. Paul, Physical aging of thin glassy polymer films monitored by gas permeability, Polymer 45 (2004) 8377–8393. doi:10.1016/j.polymer.2004.10.019.

[41] J.J. Bozzola, L.D. Russell, Electron Microscopy: Principles and Techniques for Biologist, 2nd ed., Jones and Bartlett, 1999.

[42] Rasband, W.S., ImageJ, U. S. National Institutes of Health, Bethesda, Maryland, USA, http://imagej.nih.gov/ij/, 1997-2014.

[43] X. Zhang, D.G. Cahill, O. Coronell, B.J. Mariñas, Absorption of water in the active layer of reverse osmosis membranes, J. Memb. Sci. 331 (2009) 143–151. doi:10.1016/j.memsci.2009.01.027.

[44] V. Kolev, V. Freger, Hydration, porosity and water dynamics in the polyamide layer of reverse osmosis membranes: A molecular dynamics study, Polymer 55 (2014) 1420–1426. doi:10.1016/j.polymer.2013.12.045.

[45] S. Jeck, P. Scharfer, W. Schabel, M. Kind, Water sorption in poly(vinyl alcohol) membranes: An experimental and numerical study of solvent diffusion in a crosslinked polymer, Chem. Eng. Process. Process Intensif. 50 (2011) 543–550. doi:10.1016/j.cep.2010.09.004.

[46] E. Dražević, K. Košutić, V. Freger, Permeability and selectivity of reverse osmosis membranes: Correlation to swelling revisited, Water Res. 49 (2014) 444–452. doi:10.1016/j.watres.2013.10.029.

[47] H.-J. Butt, K. Graf, M. Kappl, Physics and Chemistry of Interfaces, Wiley-VCH, Germany, 2003.

[48] R. Evans, U.M. Bettolo Marconi, P. Tarazona, Capillary Condensation and Adsorption in Cylindrical and Slit-like Pores, J. Chem. Soc., Faraday Trans. 82 (1986) 1763–1787.

[49] A. Ben-David, Y. Oren, V. Freger, Thermodynamic factors in partitioning and rejection of organic compounds by polyamide composite membranes., Environ. Sci. Technol. 40 (2006) 7023–8.

[50] P.E. Ciddor, Refractive index of air: new equations for the visible and near infrared, Appl. Opt. 35 (1996) 1566–1573.

[51] M.M. Braun, L. Pilon, Effective optical properties of non-absorbing nanoporous thin films, Thin Solid Films. 496 (2006) 505–514. doi:10.1016/j.tsf.2005.08.173.

[52] C.Y. Tang, Y.-N. Kwon, J.O. Leckie, Characterization of humic acid fouled reverse osmosis and nanofiltration membranes by transmission electron microscopy and streaming potential measurements, Environ. Sci. Technol. 41 (2007) 942–949. doi:10.1021/es061322r.

[53] S. Bason, V. Freger, Phenomenological analysis of transport of mono- and divalent ions in nanofiltration, J. Memb. Sci. 360 (2010) 389–396. doi:10.1016/j.memsci.2010.05.037.

[54] M. Ding, A. Ghoufi, A. Szymczyk, Molecular simulations of polyamide reverse osmosis membranes, Desalination. 343 (2014) 48–53. doi:10.1016/j.desal.2013.09.024.

[55] M. Ding, A. Szymczyk, F. Goujon, A. Soldera, A. Ghoufi, Structure and dynamics of water confined in a polyamide reverse-osmosis membrane: A molecular-simulation study, J. Memb. Sci. 458 (2014) 236–244. doi:10.1016/j.memsci.2014.01.054.

[56] E. Harder, D.E. Walters, Y.D. Bodnar, R.S. Faibish, B. Roux, Molecular dynamics study of a polymeric reverse osmosis membrane, J. Phys. Chem. B. 113 (2009) 10177–10182. doi:10.1021/jp902715f.

[57] M.J. Kotelyanskii, N.J. Wagner, M.E. Paulaitis, Molecular dynamics simulation study of the mechanisms of water diffusion in a hydrated, amorphous polyamide, Comput. Theor. Polym. Sci. 9 (1999) 301–306. doi:10.1016/S1089-3156(99)00020-3.

[58] A. Yaroshchuk, X. Martínez-Lladó, L. Llenas, M. Rovira, J. de Pablo, Solution-diffusion-film model for the description of pressure-driven trans-membrane transfer of electrolyte mixtures: One dominant salt and trace ions, J. Memb. Sci. 368 (2011) 192–201. doi:10.1016/j.memsci.2010.11.037.

[59] M.J. Kotelyanskii, N.J. Wagner, M.E. Paulaitis, Atomistic simulation of water and salt transport in the reverse osmosis membrane FT-30, J. Memb. Sci. 139 (1998) 1–16.

[60] D.R. Paul, Reformulation of the solution-diffusion theory of reverse osmosis, J. Memb. Sci. 241 (2004) 371–386. doi:10.1016/j.memsci.2004.05.026.

[61] B. Mi, B.J. Mariñas, D.G. Cahill, RBS characterization of arsenic(III) partitioning from aqueous phase into the active layers of thin-film composite NF/RO membranes, Environ. Sci. Technol. 41 (2007) 3290–3295.

[62] E. Drazevic, S. Bason, K. Kosutic, V. Freger, Enhanced partitioning and transport of phenolic micropollutants within polyamide composite membranes, Environ. Sci. Technol. 46 (2012) 3377–3383. doi:10.1021/es204188j.

[63] C. Maxwell, Treatise on Electricity and Magnetism, vol. 1, Oxford University Press, London, UK, 1973.

[64] L.G. Longsworth, The mutual diffusion of light and heavy water, J. Phys. Chem. 64 (1960) 1914–1917.

Graphical Abstract

Water-filled voids account for a significant volume fraction (15-32%) of polyamide active layers

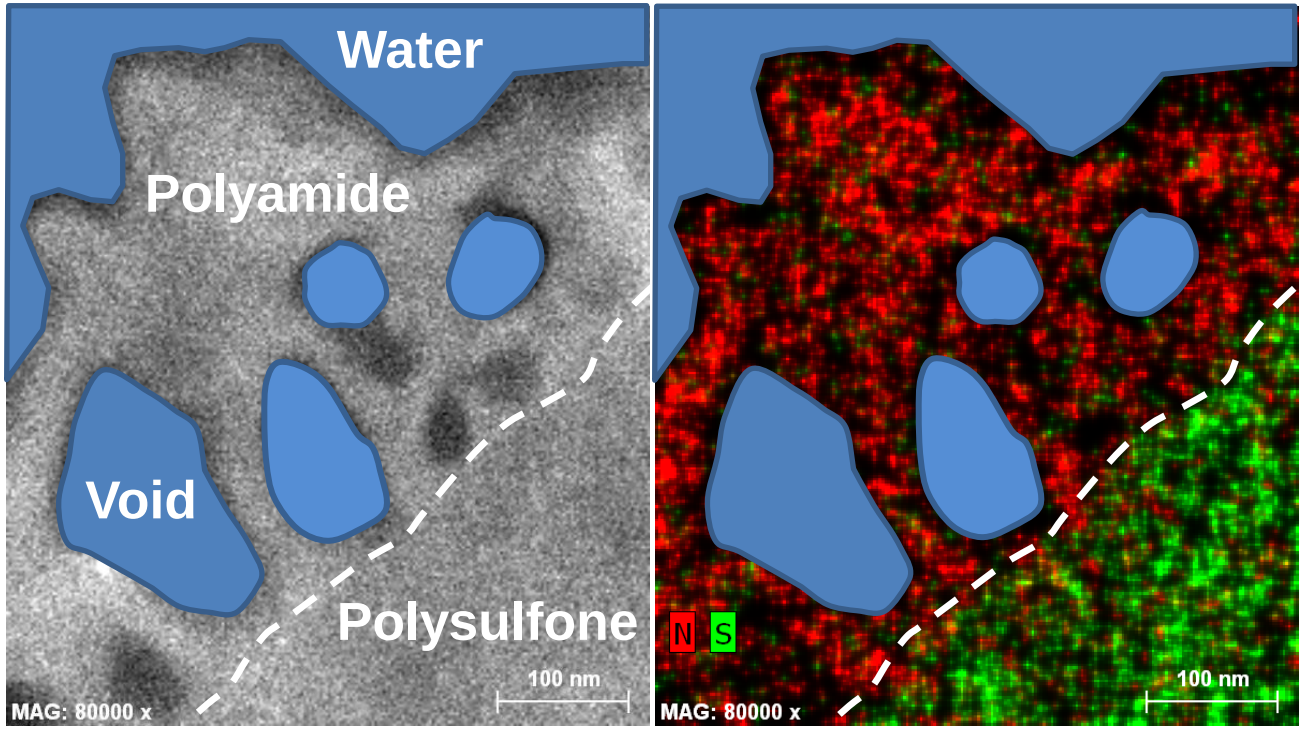

TEM image 100 nm

EDS map N S